




RESEARCH ARTICLE | OCTOBER 04 2023

The effect of instrument inertia on the initiation of oscillatory flow in stress controlled rheometry

Adeniyi Ogunkeye ; Rebecca E. Hudson; Daniel J. Curtis  



J. Rheol. 67, 1175–1187 (2023)
<https://doi.org/10.1122/8.0000665>



CrossMark

Related Content

Probing nonlinear rheology with inertio-elastic oscillations

Journal of Rheology (July 2008)

Characterizing the Non-Linear Rheology of Biopolymer Networks Using Inertio-Elastic Oscillations

AIP Conference Proceedings (July 2008)

Instabilities in stagnation point flows of polymer solutions

Physics of Fluids (August 2013)



Advance your science, career
and community as a member of
The Society of Rheology

LEARN MORE





The effect of instrument inertia on the initiation of oscillatory flow in stress controlled rheometry

Adeniyi Ogunkeye, Rebecca E. Hudson, and Daniel J. Curtis^{a)}

Complex Fluids Research Group, Department of Chemical Engineering, Faculty of Science and Engineering, Swansea University Bay Campus, Fabian Way, Swansea SA1 8EN, United Kingdom

(Received 17 March 2023; final revision received 5 September 2023; published 4 October 2023)

Abstract

In a recent paper [Hassager, J. Rheol. **64**, 545–550 (2020)], Hassager performed an analysis of the start up of stress-controlled oscillatory flow based on the general theory of linear viscoelasticity. The analysis provided a theoretical basis for exploring the establishment of a steady strain offset that is inherent to stress controlled oscillatory rheometric protocols. However, the analysis neglected the impact of instrument inertia on the establishment of the steady periodic response. The inclusion of the inertia term in the framework is important since it (i) gives rise to inertio-elastic ringing and (ii) introduces an additional phase shift in the periodic part of the response. Herein, we modify the expressions to include an appropriate inertial contribution and demonstrate that the presence of the additional terms can have a substantial impact on the time scale required to attain the steady state periodic response. The analysis is then applied to an aqueous solution of wormlike micelles. © 2023 Author(s). All article content, except where otherwise noted, is licensed under a Creative Commons Attribution (CC BY) license (<http://creativecommons.org/licenses/by/4.0/>). <https://doi.org/10.1122/8.0000665>

I. INTRODUCTION

One of the most common experimental protocols for probing the linear viscoelastic properties of complex fluids involves the use of small amplitude oscillatory shear flows to determine the storage and loss moduli [$G'(\omega)$ and $G''(\omega)$, respectively], as a function of angular frequency, ω . Such experiments can be conducted under controlled stress or controlled strain conditions. Historically, the choice of which approach to employ was determined by the type of rheometer available—those with separate motor and transducer (SMT, also known as the dual head, i.e., DH rheometers) being more suited to strain controlled experiments while those with a combined motor and transducer (CMT, also known as the single head, i.e., SH rheometers) were more suited to stress controlled experiments. Modern rheometers have sophisticated control schemes, and it is often possible to perform either type of experiment on either type of instrument. Some materials, especially those that display evolving rheological properties are often more conveniently studied using stress controlled experiments since changes in their linear viscoelastic limit can, to some extent, be naturally accounted for during the experiment. Under strain controlled conditions a small amplitude oscillatory shear waveform with amplitude γ_0 [which is, by definition, selected such that both $G'(\omega)$ and $G''(\omega)$ are independent of strain amplitude, i.e., γ_0 is within the linear viscoelastic region (the LVR) of the material] is applied to the material such that $\gamma(t) = \gamma_0 \sin(\omega t)$, which, by

definition, oscillates around the zero strain condition. The stress response to this waveform is also sinusoidal (provided that the strain amplitude is within the LVR) and takes the form

$$\sigma(t) = \gamma_0(G' \sin(\omega t) + G'' \cos(\omega t)), \quad (1)$$

thus allowing the parameters $G'(\omega)$ and $G''(\omega)$ to be determined via cross correlation or Fourier analysis.

Under stress controlled conditions (which is the focus of the present work), the initial strain response to the applied oscillatory stress consists of a periodic response, a transient response, and a strain offset [1]. In a standard stress controlled small amplitude oscillatory shear (SAOS) experiment, the periodic response is isolated by (i) introducing a “conditioning time” during which the transient part of the response decays to a negligible magnitude and which is omitted from data analysis and (ii) removing the strain offset as part of the post-processing algorithms, either by Fourier transform (where it would appear as the DC offset term) or by baseline subtraction where cross correlation based algorithms are used. Motivated by the recent work of Lee *et al.* [2] who demonstrated the utility of the strain offset in probing the zero shear viscosity, Hassager [1] derived expressions for the offset, transient and periodic contributions to the total strain for the generalized Maxwell fluid. However, this analysis neglected the impact of instrument inertia on the strain waveforms. The impact of instrument inertia on stress controlled experiments is perhaps most clearly seen in the context of a creep experiment where the coupling of the material’s elasticity and the rheometer inertia (i.e., the total system inertia inclusive of the geometry inertia, which is often calibrated

05 October 2023 12:42:12

^{a)} Author to whom correspondence should be addressed; electronic mail: d.j.curtis@swansea.ac.uk

separately) gives rise to inertio-elastic ringing at short times, i.e., free oscillations that appear superimposed upon the expected creep curve. Useful information can be extracted from such creep-ringing effects [3–7] but, in the context of an oscillatory shear experiment performed on a combined motor transducer (CMT) type rheometer, careful correction of instrument inertia artifacts is required [7,8].

Expressions for the evolution of the strain following the sudden imposition of steady stress (i.e., a creep experiment) in the presence of instrument inertia for several models can be found in the literature [3–6,9,10]. Baravian *et al.* [9] considered the onset of stress controlled flows (both creep and forced oscillation) for the Jeffrey’s fluid (which can be represented as a Voigt element in series with a viscous “dashpot”) in the presence of instrument inertia and found that, for both flows, the inertial term gave rise to a transient contribution to the total strain taking the form of a damped oscillation decaying with e^{-t/λ_2} , where λ_2 denotes the retardation time of the Voigt element [9]. The analysis of Baravian *et al.* [9] for forced (stress controlled) oscillations results in an expression for the strain evolution, $\gamma(t)$, which only contains transient and periodic contributions; the offset, which is often observed in experimental data [2], and which appears in Hassager’s analysis of the generalized Maxwell fluid [1], is absent. Lauger and Stettin also considered the impact of both sample and fluid inertia on steady state oscillatory shear in rotational rheometers, demonstrating the dramatic influence these phenomena can have on the experimental data [11].

In the present work, we extend the analysis of Hassager [1] to include the effects of instrument inertia and examine its effect on the evolution of the strain waveform as it approaches steady state conditions in stress controlled oscillatory experiments. Finally, we demonstrate the use of the analysis in a wormlike micellar system of cetylpyridinium chloride (CPyCl) and sodium salicylate (NaSal).

II. MODELING

A. Start up of oscillatory shear

Unlike dual head (DH) rheometers, in which the torque sensing element of the geometry is separated from that which is driven by the motor, torque sensing in single head (SH) rheometers occurs at the moving element of the geometry (which is undergoing continuous acceleration in oscillatory flows). Hence, both the sample and instrument inertia contribute to the total stress recorded by the instrument. Sample inertia is deemed to be negligible in the limit of gap loading [12], in which a constant velocity gradient is established within the rheometer gap, which is often assumed in rheometric experiments. The assumption of “gap loading” can be confirmed by ensuring that the rheometer gap h is much smaller than the wavelength of the propagating wave (l) with $h < l/10$ usually being considered acceptable. The reader is referred to Ewoldt *et al.* [7] (and references therein) and Lauger and Stennin (2016) [11] for further information concerning sample inertia. In the present study, we restrict attention to the gap loading condition for which the total stress (σ_t) can be expressed as the sum of the sample stress, σ_s and

the inertial stress as follows [13]:

$$\sigma_t = \sigma_s + I\ddot{\gamma}, \quad (2)$$

where I is the calibrated system inertia constant (with units Pa s^2) and $\ddot{\gamma}$ denotes the second derivative of the strain (with respect to time, t).

Noting that the Boltzmann superposition principle expresses the sample stress, σ_s , as a convolution of the stress relaxation modulus $G(t)$ and the deformation history $\dot{\gamma}$,

$$\sigma_s = \int_{-\infty}^t G(t-t')\dot{\gamma}(t') dt', \quad (3)$$

where the integral is performed over all previous times t' , we can write

$$\sigma_t = \int_{-\infty}^t G(t-t')\dot{\gamma}(t') dt' + I\ddot{\gamma}. \quad (4)$$

Or, equivalently, we can express Eq. (4) in Laplace space using the following transformations (where s denotes the independent variable in Laplace space):

$$x(s) = \int_0^{\infty} e^{-st}\sigma_t(t) dt, \quad (5)$$

$$g(s) = \int_0^{\infty} e^{-st}G(t) dt, \quad (6)$$

$$y(s) = \int_0^{\infty} e^{-st}\gamma(t) dt, \quad (7)$$

$$\dot{\gamma}(s) = sy(s), \quad (8)$$

$$\ddot{\gamma}(s) = s^2y(s), \quad (9)$$

as

$$y(s) = \frac{1}{s} \frac{x(s)}{(g(s) + Is)}. \quad (10)$$

Note that Eqs. (8) and (9) make use of the initial conditions $\gamma(0) = 0$ and $\dot{\gamma}(0) = 0$.

For a sinusoidal applied stress of amplitude σ_0 and frequency ω , which is initiated at time zero, we can write

$$\sigma_t(t) = \sigma_0 H(t) \sin(\omega t + \psi), \quad (11)$$

where $H(t)$ denotes a Heaviside step function and ψ is the initial phase of the perturbation waveform ($\psi = 0$ for a sine perturbation and $\psi = \pi/2$ for a cosine perturbation). We retain ψ for completeness but will later restrict our attention to the case of $\psi = 0$. Hence, via transformation (5), we can

write

$$x(s) = \frac{\sigma_0}{s^2 + \omega^2} (\omega \cos \psi + s \sin \psi), \quad (12)$$

which, when substituted into Eq. (10), leads to the following expressions for $y(s)$:

$$y(s) = \frac{\sigma_0(\omega \cos \psi + s \sin \psi)}{s(g(s) + Is)(s^2 + \omega^2)}. \quad (13)$$

The expression for the evolution of $\gamma(t)$ following initiation of the sinusoidal driving stress can hence be determined via the inverse Laplace transform of Eq. (13). The inverse Laplace transform may be obtained by considering the poles of Eq. (13). The expression for $\gamma(t)$ will contain three components, (i) a strain offset, γ_{off} , associated with the pole at $s = 0$; (ii) a periodic response, $\gamma_p(t)$, associated with the pole at $s = i\omega$; and (iii) a transient component, $\gamma_t(t)$, associated with the zeros of the function $g(s) + Is$. We now treat each component in turn.

First, the contribution to $\gamma(t)$ from the pole at $s = 0$ can be determined by noting that $g(0) = \eta_0$ (where η_0 denotes the zero shear viscosity) and applying the final value theorem [14],

$$\lim_{t \rightarrow \infty} \gamma(t) = \lim_{s \rightarrow 0} s y(s) \quad (14)$$

such that

$$\gamma_{off} = \frac{\sigma_0 \cos(\psi)}{\eta_0 \omega}, \quad (15)$$

which is the same as the expression for γ_{off} derived by Hassager for the inertialess condition, confirming that the strain offset is unaffected by the presence of instrument inertia.

We now consider the periodic contribution to the signal ($s = i\omega$) by evaluating $f(s) = (\omega^2 + s^2)y(s)$ at the point $s = i\omega$,

$$f(i\omega) = \frac{\sigma_0(\omega \cos \psi + i\omega \sin \psi)}{i\omega(g(s) + Ii\omega)} = \frac{\sigma_0\omega(\cos \psi + i \sin \psi)}{i\omega g(i\omega) - I\omega^2}. \quad (16)$$

Noting that the complex modulus $G^*(\omega)$ is defined as

$$G^*(\omega) = i\omega \int_0^\infty G(t) e^{-i\omega t} dt = i\omega g(i\omega), \quad (17)$$

we can write Eq. (16) as

$$f(i\omega) = \frac{\sigma_0\omega(\cos \psi + i \sin \psi)}{G^*(\omega) - I\omega^2}. \quad (18)$$

We can resolve $G^*(\omega)$ into its real and imaginary parts $G'(\omega)$ and $G''(\omega)$, the well-known storage and loss moduli,

respectively, to obtain

$$f(i\omega) = \frac{\sigma_0\omega(\cos \psi + i \sin \psi)}{(G'(\omega) - I\omega^2) + iG''(\omega)}. \quad (19)$$

Multiplying top and bottom by the complex conjugate of the denominator, we arrive at expressions for the real and imaginary parts of f as follows:

$$f_r = \frac{\sigma_0\omega((G' - I\omega^2) \cos \psi + G'' \sin \psi)}{(G' - I\omega^2)^2 + G''^2}, \quad (20)$$

$$f_i = \frac{\sigma_0\omega((G' - I\omega^2) \sin \psi - G'' \cos \psi)}{(G' - I\omega^2)^2 + G''^2}. \quad (21)$$

In Eqs. (20) and (21), we have dropped the notation $G'(\omega)$ in favor of the simpler G' , however, $G'(\omega)$ is implied.

Hence, the contribution from the poles ($s = i\omega$) can be expressed as

$$\gamma_p(t) = \frac{\sigma_0[(G' - I\omega^2) \sin(\psi + \omega t) - G'' \cos(\psi + \omega t)]}{(G' - I\omega^2)^2 + G''^2}. \quad (22)$$

Noting that while the complex compliance and complex moduli are related through the relation $J^* = 1/G^*$, their real and imaginary components are related through the expressions [15]

$$J' = \frac{G'}{G'^2 + G''^2} \quad (23)$$

and

$$J'' = \frac{G''}{G'^2 + G''^2}. \quad (24)$$

We see that for the inertia-less condition ($I = 0$), Eqs. (20) and (21) reduce to Eqs. (13) and (14) of Hassager's analysis [1], i.e.,

$$f_r = \sigma_0\omega(J' \cos \psi + J'' \sin \psi), \quad (25)$$

$$f_i = \sigma_0\omega(J' \sin \psi - J'' \cos \psi). \quad (26)$$

We now turn our attention to the poles associated with the roots of the term $g(s) + Is$, which appears in the denominator of Eq. (13). For the inertialess case, the function $g(s)$ has singularities associated with each relaxation time τ_i , (at $s = -\frac{1}{\tau_i}$) with one root [i.e., a pole of $y(s)$] intermediate between these singularities, which corresponds to the retardation times λ_j of the multimode spectrum [1] (occurring at $s = -\frac{1}{\lambda_j}$). However, in the presence of inertia, for the two mode Maxwell model, we will find that the single root is replaced by three (potentially complex) roots, which we denote ρ_k , where $k = 1, 2, 3$. As for the inertia-less case, the numerical

values of these (potentially complex valued) roots define the timescale and nature of the transient response of the system (complex conjugate roots giving rise to inertio-elastic ringing). To determine the values of ρ_k , we begin by expressing the function $g(s) + Is$ as

$$\frac{\eta_1}{1 + s\tau_1} + \frac{\eta_2}{1 + s\tau_2} + Is, \quad (27)$$

which we can equate to zero and re-write as

$$(\eta_1)(1 + s\tau_2) + (\eta_2)(1 + s\tau_1) + Is(1 + s\tau_2)(1 + s\tau_1) = 0. \quad (28)$$

Expanding Eq. (28), we find a 3rd order polynomial ($as^3 + bs^2 + cs + d = 0$) with coefficients

$$\begin{aligned} a &= I\tau_1\tau_2, \\ b &= I(\tau_1 + \tau_2), \\ c &= \tau_1\eta_2 + \tau_2\eta_1 + I, \\ d &= \eta_1 + \eta_2, \end{aligned} \quad (29)$$

the roots of which can easily be found numerically. In Fig. 1, the behavior of the functions $g(s)$ and $g(s) + Is$ between the singularities are shown graphically (in which the two mode Maxwell model has been parameterized such that the function $g(s) + Is$ has three real roots, for the ease of presentation).

Having found the roots of the function $p(s) = g(s) + Is$, which appears in the denominator of (13), we now expand $p(s)$ around the root to give

$$p(s) = (s - \rho_k)p'(\rho_k), \quad (30)$$

where

$$p'(\rho_k) = I - \sum_i \frac{\eta_i\tau_i}{(1 + \rho_k\tau_i)^2} \quad (31)$$

and hence, the contribution to $y(s)$ corresponding to the three poles can be determined by taking the sum of the residuals of $y(s)\exp(st)$ evaluated at each pole,

$$y_i(t) = \sum_k \frac{\sigma_0(\omega \cos \phi + \rho_k \sin \phi)\exp(\rho_k t)}{\rho_k \left(I - \sum_i \frac{\eta_i\tau_i}{(1 + \rho_k\tau_i)^2} \right) (\rho_k^2 + \omega^2)}. \quad (32)$$

The strain profile can then be expressed as the sum of the offset, transient, and periodic parts,

$$\gamma(t) = \gamma_{off} + \gamma_t(t) + \gamma_p(t). \quad (33)$$

B. Frequency dependency

Figures 2–4 show normalized strain profiles [normalized by the peak periodic strain, $\sigma_0/G^*(\omega)$] for the start-up of stress controlled oscillatory shear in the presence and absence of inertia for three frequency ranges denoted as

low, intermediate, and high, respectively. The designation of a frequency as low, intermediate, or high is made based on the transient part of the strain profile. Frequencies at which the transient is negligible may be considered “low frequency,” frequencies at which there is an observable transient that decays to negligible magnitude within a single period of the applied oscillation to be “mid-frequency,” and frequencies for which the transient response persists beyond a single period to be “high frequency” waveforms. We also compute a viscosity weighted average relaxation time ($\bar{\tau} = [\eta_1\tau_1 + \eta_2\tau_2]/\eta_0$) and use this to define an appropriate Deborah number ($De = \bar{\tau}\omega$). In terms of this Deborah number, the high frequency range corresponds approximately to frequencies for which $De > 10$ while the low frequency range corresponds approximately to $De < 1$.

It is also interesting to note that the amplitude of the periodic signal decreases in the high frequency range since most of the applied torque is used to accelerate the geometry/instrument; furthermore, a resonant frequency is observed as noted by several authors [9,16] (see Fig. 5). In Figs. 2–4, a spectrum with $\tau_1 = 0.01$ s, $\tau_2 = 1.0$ s, $\eta_1 = 1.0$ Pa s, $\eta_2 = 10.0$ Pa s has been employed with $I = 0.1$ Pa s². For this spectrum, the function p has one real and two complex conjugate roots leading to a damped oscillatory transient response.

C. Short time expansion and the zero frequency case

Immediately following the start-up of the stress controlled oscillatory shear, the system response will be dominated by the inertial characteristics of the instrument as discussed by Ewoldt *et al.* [4,7]. Consequently, Eq. (2) reduces to

$$\sigma_t = I\ddot{\gamma}. \quad (34)$$

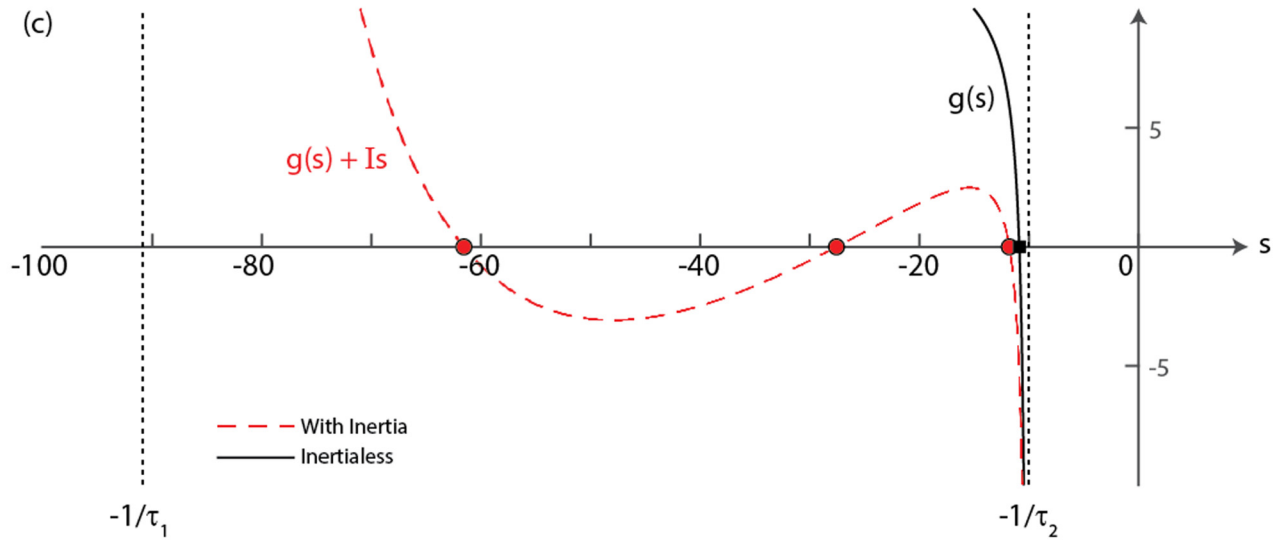
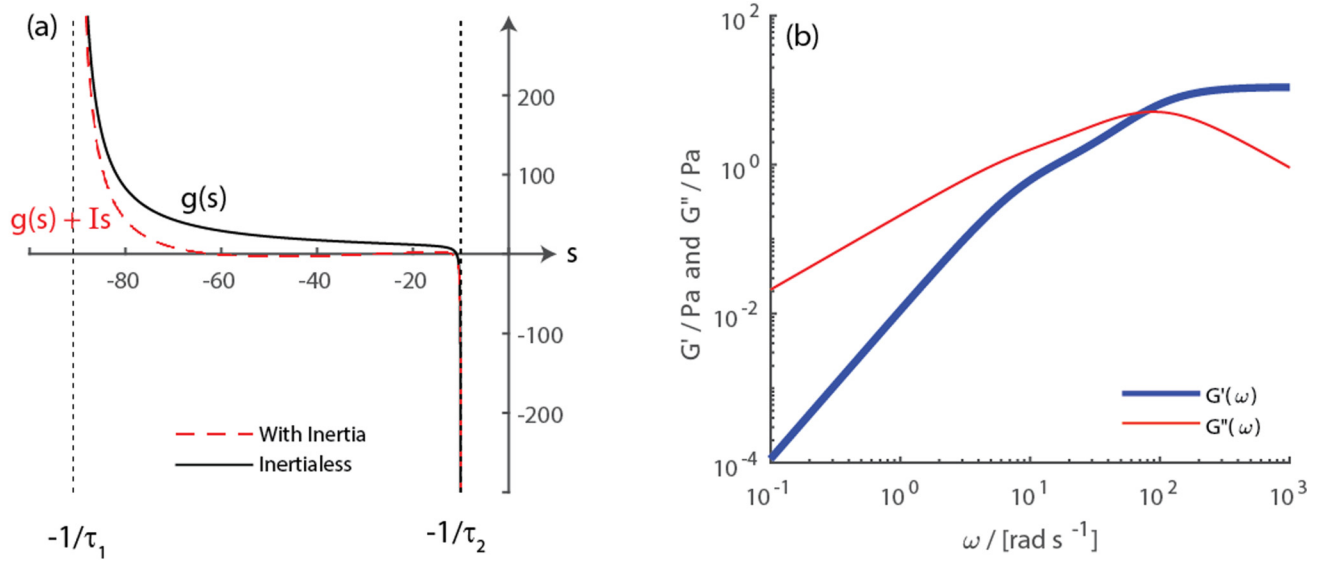
Introducing the oscillatory driving stress as $\sigma_t(t) = \sigma_0\sin(\omega t)$ and integrating results in the following expression for the initial response of the system to the onset of stress controlled oscillations,

$$\gamma(t) = \frac{\sigma_0}{\omega^2 I} [\omega t - \sin(\omega t)], \quad (35)$$

while in the zero frequency case (i.e., a creep experiment), where $\sigma(t) = \sigma_0$ for $t > 0$, integration of Eq. (34) yields a quadratic response as observed by Ewoldt *et al.* [4,7],

$$\gamma(t) = \frac{1}{2} \frac{\sigma_0}{I} t^2. \quad (36)$$

However, Eq. (33) contains the full solution for initiation of a creep style experiment as the zero frequency case with $\psi = \pi/2$. Noting that the terminal behavior of G' and G'' for a two mode Maxwell model as $\omega \rightarrow 0$ can be expressed as $(\eta_1\tau_1 + \eta_2\tau_2)\omega^2$ and $(\eta_1 + \eta_2)\omega$, respectively, we find that



05 October 2023 12:42:12

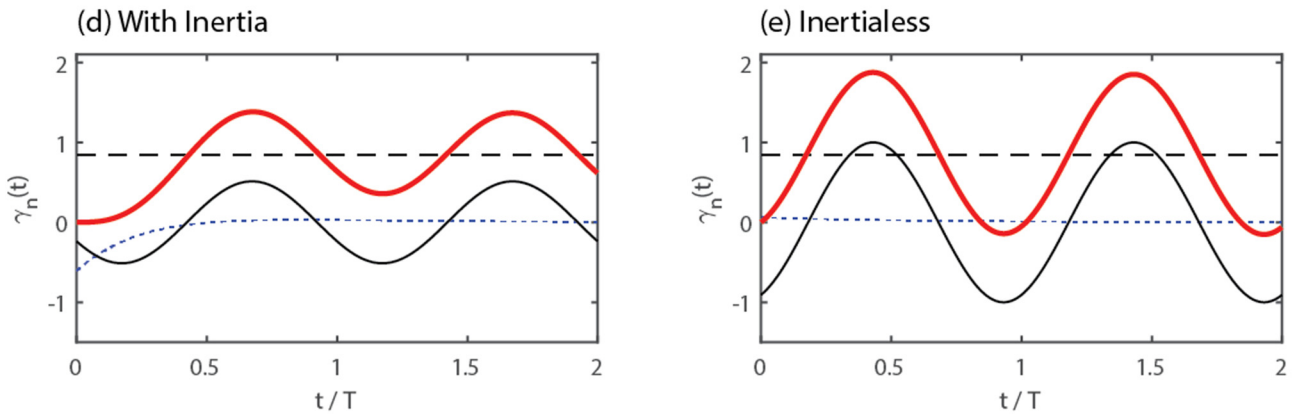


FIG. 1. (a) Comparison of the functions $g(s)$ and $g(s) + Is$ [Eq. (30)] for a two mode Maxwell model with parameters $\sigma_0 = 1 \text{ Pa}$, $\tau_1 = 0.011 \text{ s}$, $\tau_2 = 0.1 \text{ s}$, $\eta_1 = 10 \text{ Pa s}$, $\eta_2 = 1 \text{ Pa s}$, and $I = 0.5 \text{ Pa s}^2$, [$\bar{\tau} = 0.019 \text{ s}$] for which the dynamic moduli are shown in (b) (these parameters were chosen such that the characteristic polynomial of $g(s) + Is$ has three real roots). (c) shows the same data as (a) but the axis has been rescaled to show the behavior of the functions $g(s)$ and $p(s) + Is$ away from their singularities, the roots of each function are shown as filled symbols. (d) and (e) show $\gamma(t)$ in the presence and absence of inertia for $\omega = 40 \text{ rad/s}$ [$De = 0.76$], respectively, with (thick red) denoting the total strain, (thin solid black) the periodic component, (dotted) blue the transient component, and (dashed) black the strain offset component. The symbol T denotes the period of the oscillation ($2\pi/\omega$).

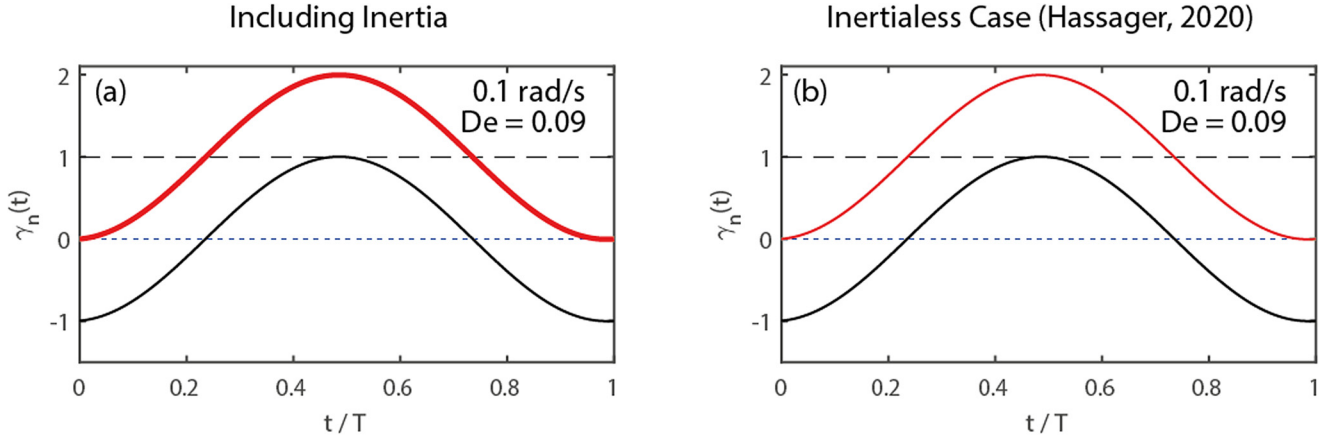


FIG. 2. Low frequency ($\omega = 0.1$ rad/s) response of a two mode Maxwell model ($\tau_1 = 0.01$ s, $\tau_2 = 1.0$ s, $\eta_1 = 1.0$ Pa s, $\eta_2 = 10.0$ Pa s, $I = 0.1$ Pa s², $[\bar{\tau} = 0.91$ s]) in the presence of instrument inertia (a) and in the inertialess [1] case (b). In both subfigures, the (thick) red line shows the complete solution, the dashed black line shows the offset (γ_{off}), the (thin) black line shows the steady state periodic response (γ_p), and the (dotted) blue line shows the transient response (γ_t). At low frequencies, including inertia in the model has negligible effect as the transient response is insignificant in comparison to the periodic and offset terms. The symbol T denotes the period of the oscillation ($2\pi/\omega$).

the limit of Eq. (33) as $\omega \rightarrow 0$ is (see the Appendix)

$$\gamma(t) = \sigma_0 \left[\frac{X - I}{\eta_0^2} + \frac{t}{\eta_0} + \sum_k \frac{\exp(\rho_k t)}{\rho_k^2 \left(I - \sum_i \frac{\eta_i \tau_i}{(1 + \rho_k \tau_i)^2} \right)} \right], \quad (37)$$

where $X = \eta_1 \tau_1 + \eta_2 \tau_2$ and $\eta_0 = \eta_1 + \eta_2$. Equation (37) is plotted in Fig. 6 along with the inertialess case [1]. From Fig. 6, it is clear that Eq. (37) includes (i) inertio-elastic ringing and (ii) an initial quadratic dependence on time associated with the acceleration of the moving geometry from rest [see Eq. (36)].

D. Generalized Maxwell model

If we consider the function $g(s)$ for a multimode Maxwell model, we find that there are singularities associated with each τ_i between which the function crosses zero only once at $s = 1/\lambda_j$, where λ_j denotes $n - 1$ retardation times. However, in the presence of inertia, we must consider the function $g(s) + Is$. The presence of the additional term ($+Is$) modifies the roots such that they no longer correspond to the retardation times of the generalized Maxwell model; instead, a triplet of roots is observed, two of which may form a complex conjugate pair (thus giving rise to inertio-elastic ringing). Each pair of relaxation times $[\tau_i, \tau_{i+1}]$ can be treated independently when determining the transient response with the discriminant of the cubic equation being used to determine the nature of the roots in the region $-1/\tau_i \leq s \leq -1/\tau_{i+1}$. Consequently, for a multimode system, we can write $\gamma(t)$ as

$$\gamma(t) = \gamma_{off} + \gamma_t(t) + \gamma_p(t), \quad (38)$$

where

$$\gamma_{off} = \frac{\sigma_0 \cos \phi}{\omega \eta_0}, \quad (39)$$

$$\gamma_p(t) = \frac{\sigma_0 [(G' - I\omega^2) \sin(\psi + \omega t) - G'' \cos(\psi + \omega t)]}{(G' - I\omega^2)^2 + G''^2}, \quad (40)$$

where

$$G'(\omega) = \sum_i \frac{\eta_i \tau_i^2 \omega^2}{1 + \tau_i^2 \omega^2}, \quad (41)$$

$$G''(\omega) = \sum_i \frac{\eta_i \tau_i \omega}{1 + \tau_i^2 \omega^2}, \quad (42)$$

and

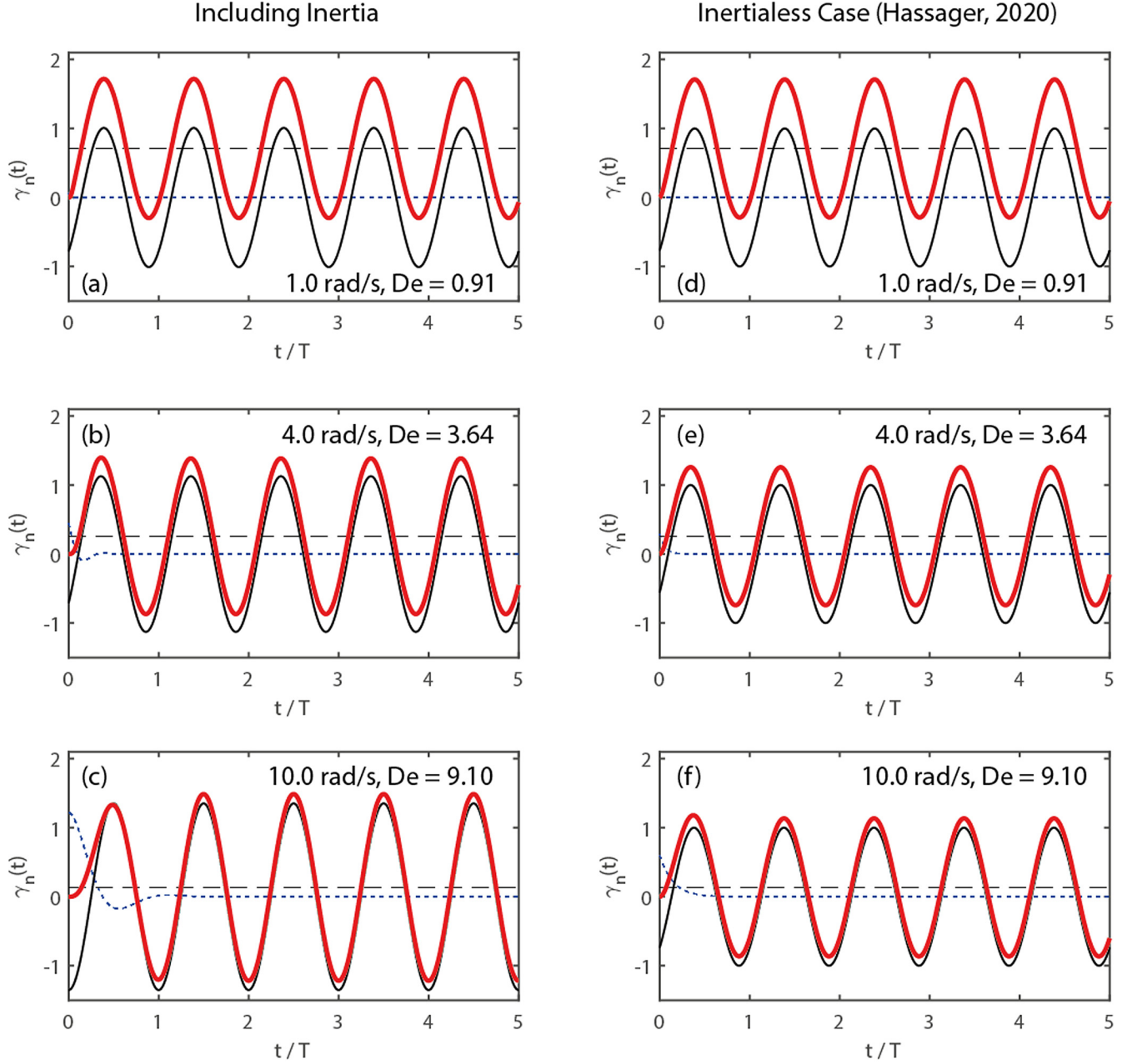
$$y_t(t) = \sum_{i=1}^{N-1} \sum_k \frac{\sigma_0 (\omega \cos \phi + \rho_{i,k} \sin \phi) \exp(\rho_{i,k} t)}{\rho_{i,k} \left(I - \frac{\eta_i \tau_i}{(1 + \rho_{i,k} \tau_i)^2} - \frac{\eta_{i+1} \tau_{i+1}}{(1 + \rho_{i,k} \tau_{i+1})^2} \right) (\rho_{i,k}^2 + \omega^2)}. \quad (43)$$

In Eq. (43), $\rho_{i,k}$ refers to the k th root of $as^3 + bs^2 + cs + d = 0$ for the pair of modes appearing at $[\tau_i, \tau_{i+1}]$. There are three roots (and hence, $k = 1, 2, 3$) if the discriminant of this polynomial (i.e., $\Delta = 18abcd - 4b^3d + b^2c^2 - 4ac^3 - 27a^2d^2$) for the pair of modes is positive (three real roots) or negative (one real and two complex conjugate roots). If the determinant evaluates to 0 the polynomial has a repeated root; a single repeated root if $3ac = b^2$ resulting in $k = 1$, otherwise, there are two roots and $k = 1, 2$. It is interesting to note that if $I = 0$ then $a = b = 0$ and the conditions for a single repeated root are satisfied. Hence, the roots of the polynomial return to the retardation times of the model as per Hassager's analysis [1].

E. Newtonian solvent

The inclusion of a Newtonian solvent (with viscosity η_s) such that the sample stress is expressed as

$$\sigma_{sample} = \int_{-\infty}^t G(t-t') \dot{\gamma}(t') dt' + I \ddot{\gamma} + \eta_s \dot{\gamma} \quad (44)$$



05 October 2023 12:42:12

FIG. 3. Intermediate frequency ($1.0 \text{ rad/s} \leq \omega \leq 10 \text{ rad/s}$) response of a two mode Maxwell model ($\tau_1 = 0.01 \text{ s}$, $\tau_2 = 1.0 \text{ s}$, $\eta_1 = 1.0 \text{ Pa s}$, $\eta_2 = 10.0 \text{ Pa s}$, $I = 0.1 \text{ Pa s}^2$, $[\bar{\tau}] = 0.91 \text{ s}$) in the presence of instrument inertia (a)–(c) and in the inertialess [1] case (d)–(f). In both subfigures, the (thick) red line shows the complete solution, the dashed black line shows the offset (γ_{off}), the (thin) black line shows the steady state periodic response (γ_p), and the (dotted) blue line shows the transient response (γ_t). As frequency increases, the effect of the transient terms becomes more important in the initial response. At these frequencies, the inclusion of inertia introduces a damped oscillatory behavior to the transient response, which decays within the period of one oscillation. The symbol T denotes the period of the oscillation ($2\pi/\omega$).

modifies Eq. (10) to

$$y(s) = \frac{1}{s} \frac{x(s)}{(g(s) + Is + \eta_s)}, \quad (45)$$

the solution of which also consists of offset, periodic, and transient components. Using a similar procedure to that reported above, the offset component of the strain profile can

be expressed as

$$\gamma_{off}(t) = \frac{\sigma_0 \cos(\psi)}{(\eta_0 + \eta_s)\omega}, \quad (46)$$

while the periodic part can be expressed as

$$\gamma_p(t) = \frac{\sigma_0 [(G^2 - I\omega^2) \sin(\psi + \omega t) - (G' + \eta_s\omega) \cos(\psi + \omega t)]}{(G' - I\omega^2)^2 + (G'' + \eta_s\omega)^2}. \quad (47)$$

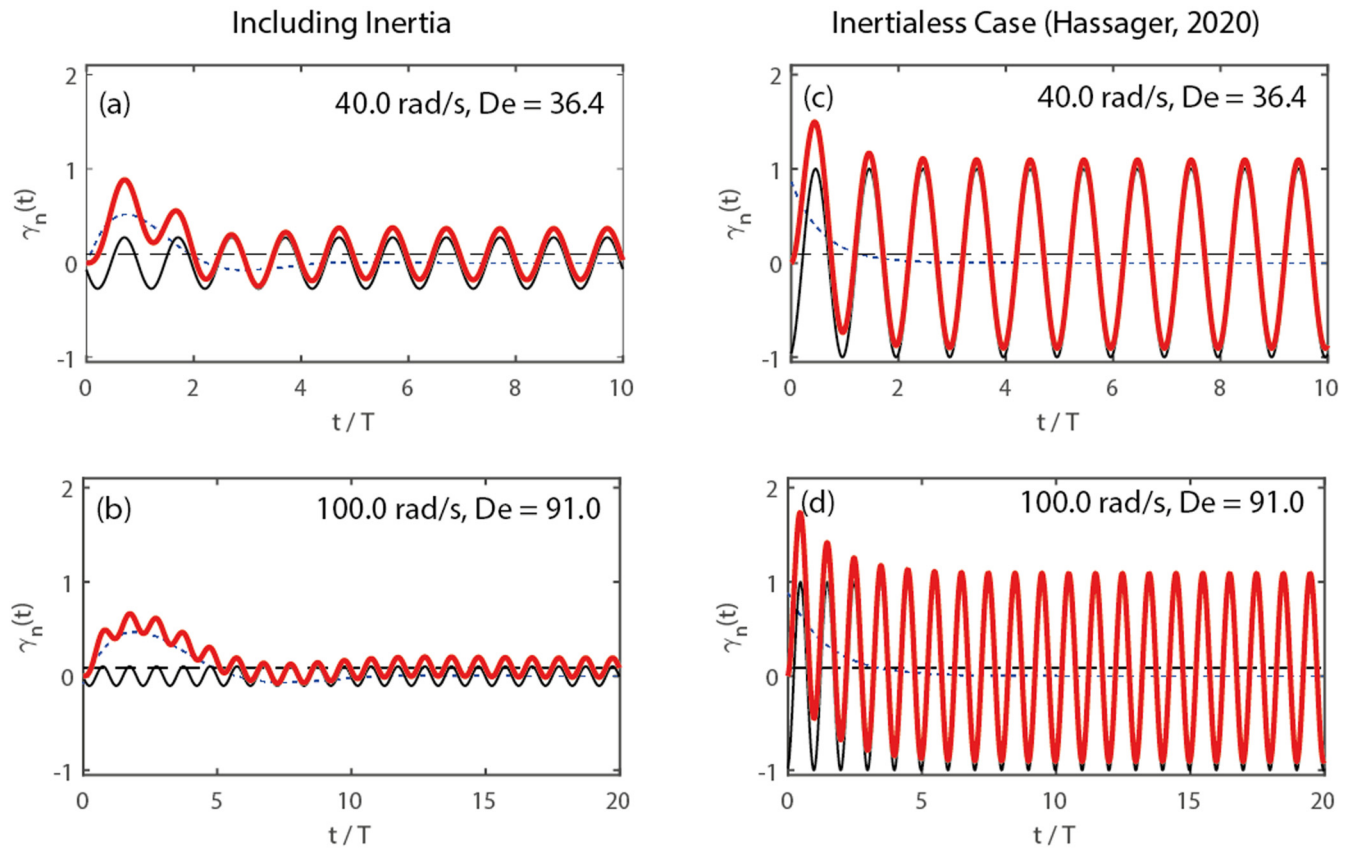


FIG. 4. High frequency ($\omega > 10$ rad/s) response of a two mode Maxwell model ($\tau_1 = 0.01$ s, $\tau_2 = 1.0$ s, $\eta_1 = 1.0$ Pa s, $\eta_2 = 10.0$ Pa s, $I = 0.1$ Pa s², $[\bar{\tau} = 0.91$ s]) in the presence of instrument inertia [(a) and (b)] and in the inertialess [1] case [(c) and (d)]. In both subfigures, the (thick) red line shows the complete solution, the dashed black line shows the offset (γ_{off}), the (thin) black line shows the steady state periodic response (γ_p), and the (dotted) blue line shows the transient response (γ_t). At these frequencies, including inertia in the model has a dramatic effect on the response, which displays damped oscillatory behavior. Here, the transient response takes longer than one period to decay to a negligible magnitude, and hence, we consider them to be “high frequencies,” special care must be taken when undertaking experiments at high frequencies with regard to (i) inertia correction and (ii) allowing a sufficient conditioning time for the transients to decay prior to data acquisition.

05 October 2023 12:42:12

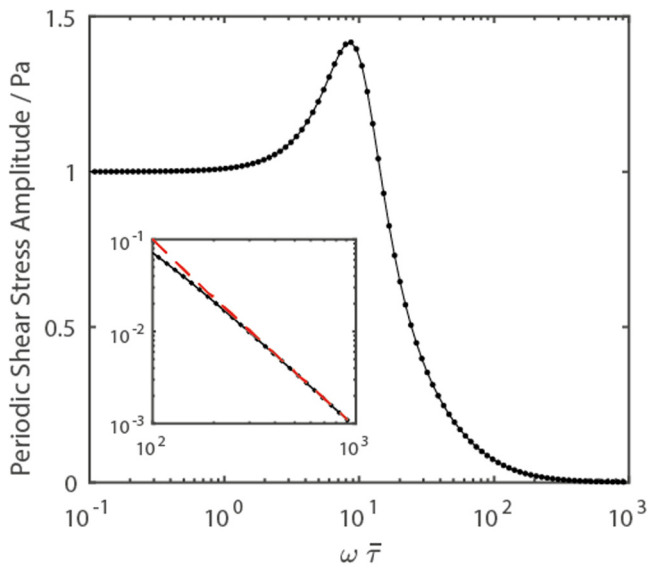


FIG. 5. Amplitude of the periodic stress component as a function of frequency for a two mode Maxwell model ($\tau_1 = 0.01$ s, $\tau_2 = 1.0$ s, $\eta_1 = 1.0$ Pa s, $\eta_2 = 10.0$ Pa s, $I = 0.1$ Pa s², $[\bar{\tau} = 0.91$ s]). The inset shows high frequency asymptotic behavior [i.e., $|G/(G - I\omega^2)|$, where $G = \eta_1/\tau_1 + \eta_2/\tau_2$].

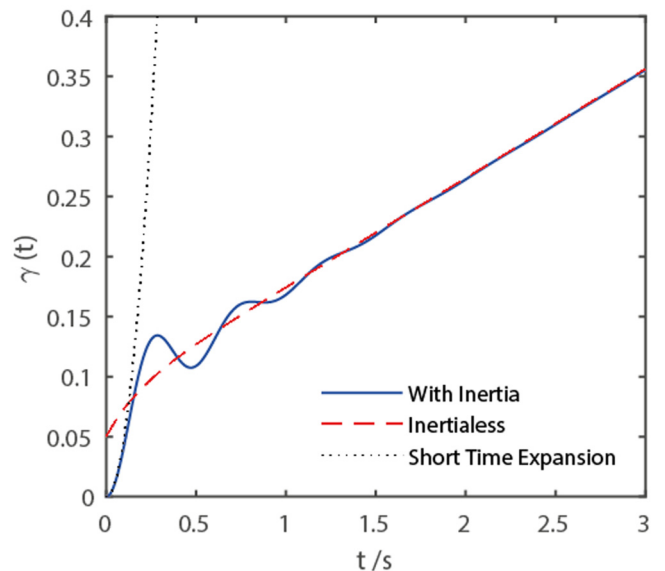


FIG. 6. Zero frequency response (i.e., start up of creep) for a two mode Maxwell model ($\tau_1 = 0.1$ s, $\tau_2 = 1.0$ s, $\eta_1 = 1.0$ Pa s, $\eta_2 = 10.0$ Pa s, $I = 0.1$ Pa s², $[\bar{\tau} = 0.92$ s]).

Finally, the transient part is determined by considering the zeros of the function $g(s) + Is + \eta_s$. For a two mode Maxwell model (with Newtonian solvent), this can be expressed as

$$\frac{\eta_1}{1 + s\tau_1} + \frac{\eta_2}{1 + s\tau_2} + Is + \eta_s, \quad (48)$$

which we can equate to zero and re-write as

$$\begin{aligned} &\eta_1(1 + s\tau_2) + \eta_2(1 + s\tau_1) + Is(1 + s\tau_2)(1 + s\tau_1) \\ &+ \eta_s(1 + s\tau_1)(1 + s\tau_2) + \eta_1(1 + s\tau_2) + \eta_2(1 + s\tau_1) \\ &+ (Is + \eta_s)(1 + s\tau_1 + s\tau_2 + s^2\tau_1\tau_2) = 0. \end{aligned} \quad (49)$$

Expanding Eq. (49) as before, we find a third order polynomial ($as^3 + bs^2 + cs + d = 0$) with coefficients

$$\begin{aligned} a &= I\tau_1\tau_2, \\ b &= I(\tau_1 + \tau_2) + \eta_s\tau_1\tau_2, \\ c &= \tau_1\eta_2 + \tau_2\eta_1 + I + \eta_s\tau_1 + \eta_s\tau_2, \\ d &= \eta_1 + \eta_2 + \eta_s. \end{aligned} \quad (50)$$

As before, the roots of the polynomial, ρ_k , can be found numerically. Expansion of the function $p(s) = g(s) + Is + \eta_s$ results in the expression

$$y_t(t) = \sum_k \frac{\sigma_0(\omega \cos \phi + \rho_k \sin \phi) \exp(\rho_k t)}{\rho_k \left(I - \sum_i \frac{\eta_i \tau_i}{(1 + \rho_k \tau_i)^2} \right) (\rho_k^2 + \omega^2)}, \quad (51)$$

which is identical to Eq. (32). As previously, the strain profile can then be expressed as the sum of the offset, transient, and periodic parts.

F. Effect of inertia on “conditioning time”

When designing stress controlled oscillatory experiments, it is important to recognize that a conditioning time (the time which is allowed to elapse between the initiation of the perturbation waveform and the collection of “periodic” data) based on an arbitrary criterion such as “the period of a single cycle” may not be sufficient. Indeed, for the inertialess case, Hassager demonstrated that the transient response decays with $\exp(-t/\lambda_k)$. A conditioning time of $\approx 4\lambda_k$ allows the transient to decay to $\approx 2\%$ of its initial magnitude. However, in Figs. 3 and 4, the transient term persists for longer in the presence of inertia than in the inertialess case for all frequencies. Plotting the three poles associated with the transient response (see Fig. 7), it can be seen that in the presence of inertia the pair of complex conjugate poles are (i) dominant over the single real pole (i.e., they appear significantly closer to the imaginary axis) and (ii) the real part of the complex conjugate pair lies to the right of the single pole of the inertialess case. The rate of decay of the transient response is predominantly determined by an effective retardation time $\lambda^* = -1/\text{Re}[\rho_k^+]$ (where ρ_k^+ refers to the dominant pole). Consequently, selection of an appropriate “conditioning time” should involve an assessment of inertio-elastic effects

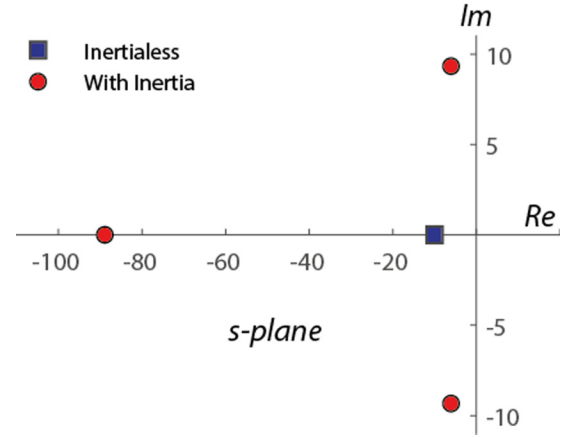


FIG. 7. Pole plot for the “inertialess” and “including inertia” cases for a two mode Maxwell model ($\tau_1 = 0.01$ s, $\tau_2 = 1.0$ s, $\eta_1 = 1.0$ Pa s, $\eta_2 = 10.0$ Pa s, $I = 0.1$ Pa s²). While the inertialess transient is characterized by a single real pole at $s = -1/\lambda_k$, inertia introduces a pair of complex conjugate poles, which dominate the transient response and generate a dominant effective retardation time λ^* .

with $t_c \approx 4\lambda^*$, allowing the transient to decay to $\approx 2\%$ of its initial magnitude. For certain relaxation spectra, the presence of inertia may accelerate the decay of the transient component. Experimentally, where the relaxation spectrum is unlikely to be known *a priori*, direct observation/analysis of the transient response may be the quickest way to determine the appropriate conditioning time.

III. EXPERIMENTS

A. Materials and methods

1. Sample preparation

Cetylpyridinium chloride (CPyCl) and sodium salicylate (NaSal) (Sigma-Aldrich) were dissolved at a molar ratio of

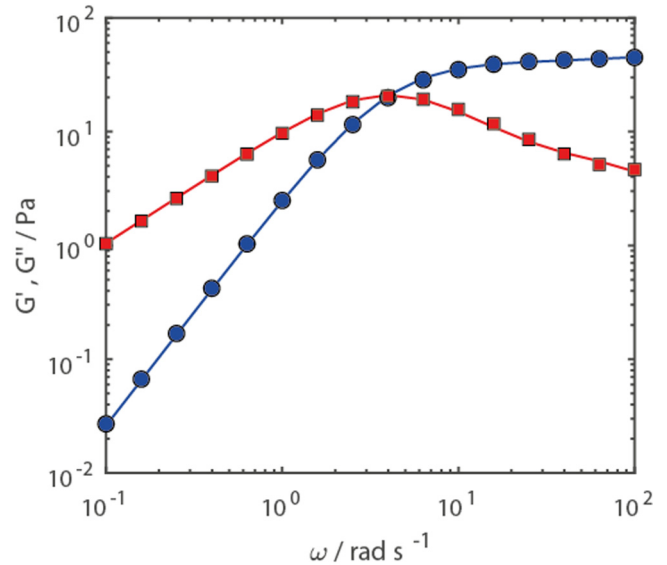


FIG. 8. $G'(\omega)$ (blue circles) and $G''(\omega)$ (red squares) data for a 4.1 wt. % solution of CPyCl and NaCl. Lines show a two mode Maxwell model fit to the experimental data with $\tau_1 = 0.251$ s, $\tau_2 = 0.013$ s, $\eta_1 = 10.37$ Pa s, $\eta_2 = 0.08$ Pa s, $[\bar{\tau} = 0.25$ s].

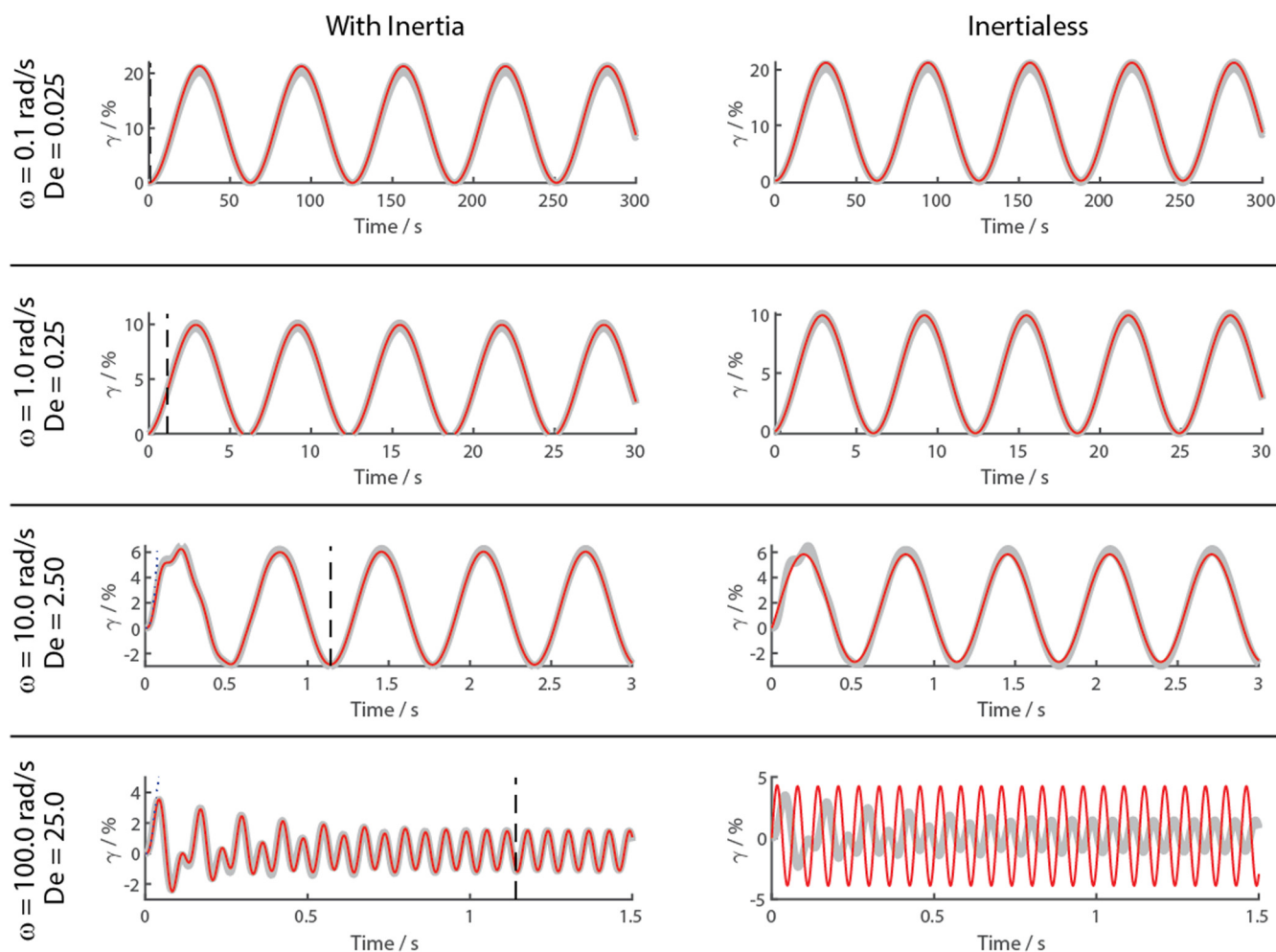


FIG. 9. Transient data for start up of stress controlled oscillatory shear for a 4.1 wt. % solution of CPyCl and NaCl at frequencies of (a) 0.1, (b) 1.0, (c) 10, and (d) 100 rad s^{-1} . Gray (light) lines show experimental data as the mean and standard deviation of three experiments. In the left hand column, the red (dark) line shows the full solution (see Sec. II A) for a two mode Maxwell model in the presence of inertia. The model has been parameterized by fitting SAOS data for the same material (see Fig. 8) with no additional free parameters involved in generating the data presented in this figure. The blue dashed lines in the 10 and 100 rad/s figures show the short time expansion result corresponding to Eq. (36). The vertical dashed lines at $t \approx 4\lambda^* \approx 1.14$ s denote the point at which the transient component of the response (with inertia) has decayed to 2% of its initial magnitude (see Sec. II F). In the right hand column, the same experimental data are shown but the red (dark) line shows the inertialess solution of Hassager [1].

2:1 in 0.5M sodium chloride (NaCl) solutions prepared using de-ionized water. Appropriate quantities of dry NaCl, NaSal, and CPyCl, in powdered form, were added to de-ionized water to generate a 4.1 wt. % solution of CpyCl in a fume hood. This concentration has previously been shown to display shear thinning (rather than shear banding) characteristics [17,18]. The mixtures were stirred for 24 h at 40 °C (in a sealed beaker atop a heated plate) to completely disperse the powder before measurements were performed. All chemicals were used as received without further purification.

2. Rheometry

Small amplitude oscillatory shear (SAOS) and start-up of stress controlled oscillations with $\psi = 0$ (referred to as “transient” experiments herein) were performed using a TA Instruments HR-30 rheometer fitted with a 60.0 mm 2° aluminum cone. The sample was loaded to the temperature controlled (Peltier) plate of the rheometer and a thin layer of low viscosity silicone oil was added to prevent evaporation. All experiments were performed at 25 °C. For transient data

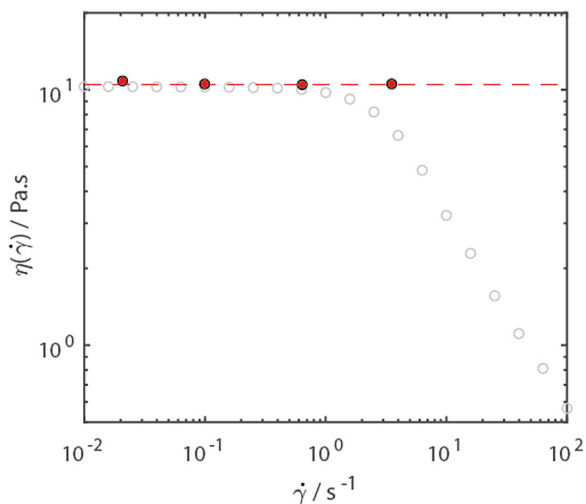


FIG. 10. Flow curve for a 4.1 wt. % Solution of CPyCl and NaCl. Gray (open) circles show experimental data. The dashed red line shows the expected zero shear viscosity predicted from the two model Maxwell model (i.e., $\eta_1 + \eta_2$, from the fit shown in Fig. 8). Red (closed) circles show the zero shear viscosity determined from the measured strain offset following Eq. (15) plotted at $\gamma_{max}\omega$ for each frequency.

collected at the two lowest frequencies (0.1 and 1.0 rad s⁻¹), it was necessary to correct the strain waveforms for strain drift. This was achieved by fitting a straight line ($y = mx + c$) to the final few peaks of the strain waveform in order to identify the drift rate (m) before subtracting the product mt from the measured strain signal. This correction was unnecessary for the higher frequencies due to the far shorter duration of data acquisition.

The moment of inertia of the instrument and geometry were determined prior to experiments using standard calibration procedures. The instrument moment of inertia constant was $M_i = 21.02 \mu\text{N ms}^2$ and the geometry moment of inertia constant was $M_g = 8.80 \mu\text{N ms}^2$. The total moment of inertia was then converted to I [as it appears in Eq. (4), with units of Pa s²] using the appropriate geometry factors [4,9] ($F_\sigma = 3/2\pi R^3$ and $F_\gamma = 1/\tan \alpha$, where R denotes the cone radius and α the cone angle) such that $I = (M_i + M_g) \times F_\sigma/F_\gamma = 0.0185 \text{ Pa s}^2$.

B. Results and discussion

Figure 8 shows SAOS data along with a two mode Maxwell model fit (with $\tau_1 = 0.251 \text{ s}$, $\tau_2 = 0.013 \text{ s}$, $\eta_1 = 10.37 \text{ Pa s}$, $\eta_2 = 0.08 \text{ Pa s}$, $[\bar{\tau} = 0.25 \text{ s}]$) which shows excellent agreement over the entire frequency range. The 2 mode model was then used to “predict” the strain profiles occurring in response to the start up of oscillatory stress controlled oscillations (at $\omega = [0.1 \text{ rad/s}, 1.0 \text{ rad/s}, 10.0 \text{ rad/s}, 100.0 \text{ rad/s}]$) in the presence and absence of inertia using Eq. (33) with $I = 0.0185 \text{ Pa s}^2$ and $I = 0 \text{ Pa s}^2$, respectively. Corresponding experimental data were also obtained at the same angular frequencies using the transient acquisition mode of the HR-30. Figure 9 shows excellent agreement between the predictions (thin red line) and experimental data (thick gray lines) at all frequencies when inertia is included within the model (left hand column). Where inertia is omitted (as per the solution of Hassager [1]), the model captures the dynamics of the strain waveform only at low frequencies, as would be

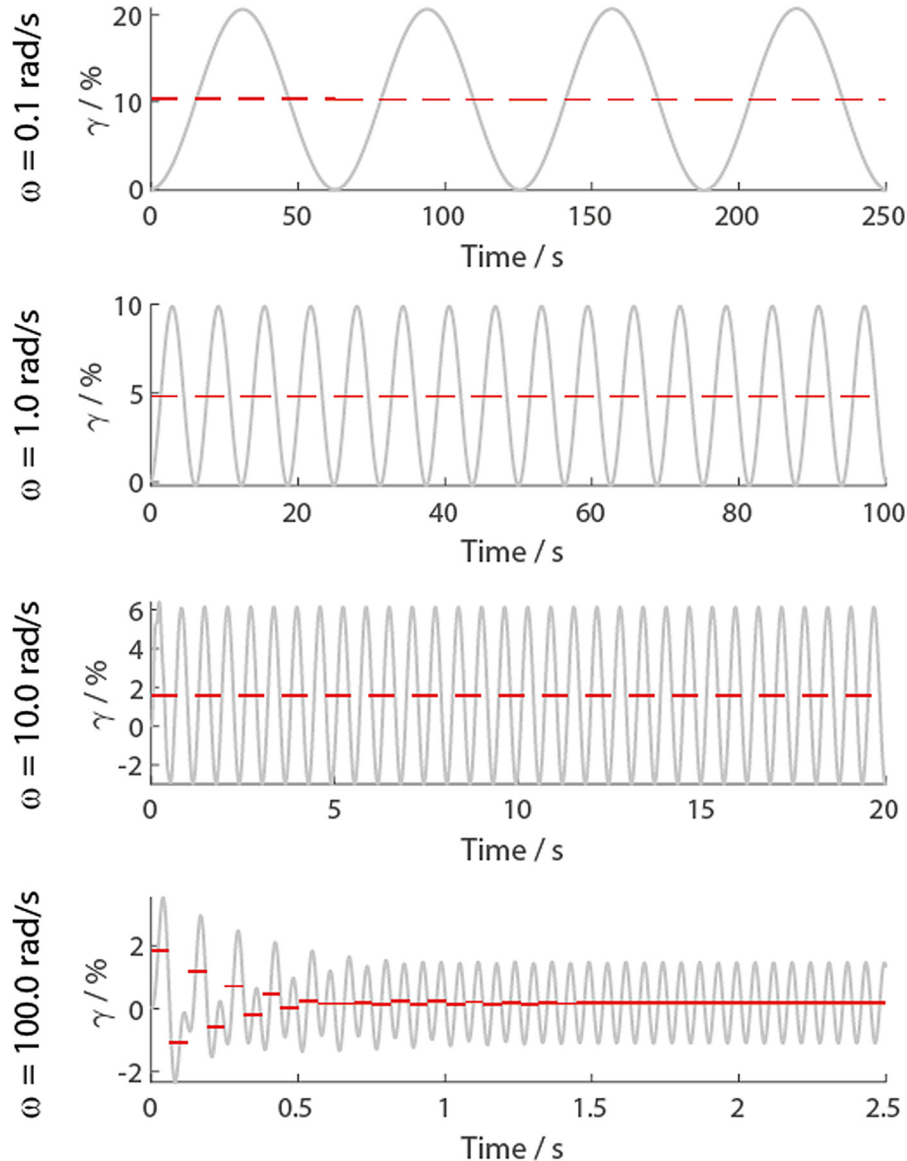


FIG. 11. Strain offset evolution. Mean strain over each cycle (dashed red line) for the experimental strain waveforms at 0.1, 1.0, 10.0, and 100.0 rad/s. In the limit of long times, the mean value across each cycle tends to a constant strain offset, which can be used to determine the zero shear viscosity via Eq. (52).

expected. At higher frequencies, the effects of (i) inertial-ringing, (ii) reduced strain amplitude due to resonance effects, and (iii) the inertial phase shift are missing. Consequently, the inertialess model is insufficient at 10 and 100 rad/s. Comparison of the measured and predicted strain waveforms in this manner establishes confidence in the data and in the discrete relaxation spectrum (DRS) fitted to the SAOS data since small errors in the dynamic moduli [$G'(\omega)$ and $G''(\omega)$] are well known to generate large deviations in the DRS.

Figure 10 shows the flow curve (gray open circles) for the WLM sample for $0.01 \leq \dot{\gamma} \leq 100 \text{ s}^{-1}$, which clearly shows a zero-shear plateau viscosity of around 10.5 Pa s. Also shown in Fig. 10 is the zero shear viscosity calculated from the two mode Maxwell model fit of Fig. 8, which shows excellent agreement with the measured flow curve data, again, establishing confidence in the ability of the two mode Maxwell model to capture the linear viscoelastic behavior of the specific WLM system studied herein. The zero shear viscosity can also be obtained from the strain offset observed in the strain profile following start up of stress controlled oscillations. As shown in Sec. II A the strain offset is unaffected by instrument inertia and hence (following Lee *et al.* [2]), the zero shear viscosity can be determined by measuring the strain offset (determined herein as the mean value of strain in the long time limit, see Fig. 11) through a simple rearrangement of Eq. (15) to

$$\eta_0 = \frac{\sigma_0 \cos(\psi)}{\gamma_{\text{off}}(\omega)\omega}. \quad (52)$$

Figure 10 shows values of η_0 determined from the strain offset at each frequency as red (filled) circles (for ease of visualization, these are plotted at $\gamma_{\text{max}}\omega$ for each frequency, where γ_{max} denotes the maximum strain observed in the waveforms). Excellent agreement is observed between values of η_0 obtained from (i) the flow curve, (ii) the two mode Maxwell model fit, and (iii) strain offsets.

IV. CONCLUSIONS

Herein, we have demonstrated how rheometer inertia (including instrument and geometry contributions) influences the establishment of the steady state periodic response to a stress controlled oscillatory perturbation in the context of the general theory of linear viscoelasticity. In contrast to the inertialess case, in which the transient terms decay exponentially with time constants set by the retardation times of the discrete spectrum [1], the presence of inertia modifies this response to include inertio-elastic ringing reminiscent of that seen in creep experiments [3–6,9,10] (which is included in the present analysis as the zero frequency case). Consequently, the timescale for the establishment of the steady state periodic response is dramatically affected by the presence of rheometer inertia. In practice, this highlights the importance of selecting an appropriate “conditioning time” when designing experimental procedures that rely on the steady state response either for direct determination of the dynamic moduli or probing the zero shear viscosity via the strain offset. Direct observation/analysis of the transient response

during preliminary experiments may be the most robust way to determine the appropriate conditioning time.

The effect of instrument inertia on experiments involving more complex waveforms, for example, stress-controlled optimally windowed chirps ($\sigma - OWCh$) [19,20] is anticipated to be more complicated and we leave the analysis of this problem to a later paper.

ACKNOWLEDGMENTS

The authors acknowledge funding from the Engineering and Physical Sciences Research Council, UK, through Grant Nos. EP/N013506/1 and EP/T026154/1 and the European Regional Development Fund via the Smart Expertise program of the Welsh Government. The authors are also grateful to Dr. Rowan Brown of Swansea University for helpful discussion.

AUTHOR DECLARATIONS

Conflict of Interest

The authors have no conflicts to disclose.

DATA AVAILABILITY

The data that support the findings of this study are available within the article.

APPENDIX: DERIVATION OF ZERO FREQUENCY RESPONSE

The zero frequency response has been derived as follows. For $\psi = \pi/2$, the offset term reduces to zero independently of ω , it hence makes no contribution to the creep response. The periodic response can be derived by firstly substituting the expressions for the terminal response of a two mode Maxwell model for $G'(\omega)$ and $G''(\omega)$, i.e., $G'(\omega) = (\eta_1 \tau_1 + \eta_2 \tau_2)\omega^2$ and $G''(\omega) = (\eta_1 + \eta_2)\omega$. To simplify the notation, let $X = (\eta_1 \tau_1 + \eta_2 \tau_2)$ and $\eta_0 = \eta_1 + \eta_2$, hence, we have

$$\gamma_p(t) = \frac{\sigma_0[(X\omega^2 - I\omega^2) \sin(\psi + \omega t) - \eta_0\omega \cos(\psi + \omega t)]}{(G\omega^2 - I\omega^2)^2 + \eta_0^2\omega^2}, \quad (A1)$$

now let $A = X - I$ such that

$$\gamma_p(t) = \frac{\sigma_0[A\omega^2 \sin(\psi + \omega t) - \eta_0\omega \cos(\psi + \omega t)]}{A^2\omega^4 + \eta_0^2\omega^2}, \quad (A2)$$

which simplifies further to

$$\gamma_p(t) = \frac{\sigma_0[A\omega^2 \sin(\psi + \omega t) - \eta_0\omega \cos(\psi + \omega t)]}{\omega^2(A^2\omega^2 + \eta_0^2)}. \quad (A3)$$

We can now separate out the terms such that

$$\gamma_p(t) = \frac{\sigma_0 A \sin(\psi + \omega t)}{A^2\omega^2 + \eta_0^2} - \frac{\sigma_0 \eta_0 \cos(\psi + \omega t)}{\omega(A^2\omega^2 + \eta_0^2)}, \quad (A4)$$

which by noting that $\cos(B + C) = \cos B \cos C - \sin B \sin C$, we can expand further to be

$$\gamma_p(t) = \frac{\sigma_0 A \sin(\psi + \omega t)}{A^2 \omega^2 + \eta_0^2} - \frac{\sigma_0 \eta_0 \cos(\psi) \cos(\omega t)}{\omega(A^2 \omega^2 + \eta_0^2)} + \frac{\sigma_0 \eta_0 \sin(\psi) \sin(\omega t)}{\omega(A^2 \omega^2 + \eta_0^2)}. \quad (\text{A5})$$

By setting $\psi = \pi/2$, the second term is removed and the expression reduces to

$$\gamma_p(t) = \frac{\sigma_0 A \sin(\pi/2 + \omega t)}{A^2 \omega^2 + \eta_0^2} + \frac{\sigma_0 \eta_0 \sin(\omega t)}{(A^2 \omega^2 + \eta_0^2) \omega}. \quad (\text{A6})$$

Finally, noting that the limit of $\sin(\omega t)/\omega$ as $\omega \rightarrow 0$ is t and setting $\omega = 0$, we find

$$\gamma_p(t) = \frac{\sigma_0 A}{\eta_0^2} + \frac{\sigma_0 t}{\eta_0} \quad (\text{A7})$$

or, in its full form

$$\gamma_p(t) = \sigma_0 \left[\frac{(X - I)}{\eta_0^2} + \frac{\sigma_0 t}{\eta_0} \right]. \quad (\text{A8})$$

The contribution from the transient parts can be determined directly by setting $\psi = \pi/2$ and substituting $\omega = 0$ in Eq. (32),

$$y_i(t) = \sum_k \frac{\sigma_0 \exp(\rho_k t)}{\rho_k^2 \left(I - \sum_i \frac{\eta_i \tau_i}{(1 + \rho_k \tau_i)^2} \right)}, \quad (\text{A9})$$

summing Eqs. (A8) and (A9) leads to the expression for start up of steady stress [i.e., Eq. (37), reproduced below for convenience],

$$\gamma(t) = \sigma_0 \left[\frac{X - I}{\eta_0^2} + \frac{t}{\eta_0} + \sum_k \frac{\exp(\rho_k t)}{\rho_k^2 \left(I - \sum_i \frac{\eta_i \tau_i}{(1 + \rho_k \tau_i)^2} \right)} \right]. \quad (\text{A10})$$

REFERENCES

- [1] Hassager, O., “Stress-controlled oscillatory flow initiated at time zero: A linear viscoelastic analysis,” *J. Rheol.* **64**(3), 545–550 (2020).
- [2] Lee, J. C.-W., Y.-T. Hong, K. M. Weigandt, E. G. Kelley, H. Kong, and S. A. Rogers, “Strain shifts under stress-controlled oscillatory shearing in theoretical, experimental, and structural perspectives: Applications to probing zero-shear viscosity,” *J. Rheol.* **63**, 863–881 (2019).
- [3] Baravian, C., and D. Quemada, “Using instrumental inertia in controlled stress rheometry,” *Rheol. Acta* **37**, 223–233 (1998).
- [4] Ewoldt, R. H., and G. H. McKinley, “Creep ringing in rheometry,” *Rheol. Bull.* **76**, 4–24 (2007).
- [5] Yao, N. Y., R. J. Larson, and D. A. Weitz, “Probing nonlinear rheology with inertio-elastic oscillations,” *J. Rheol.* **52**, 1013–1025 (2008).
- [6] Joshi, Y. M., G. R. Reddy, A. L. Kulkarni, N. Kumar, and R. P. Chhabra, “Rheological behaviour of aqueous suspensions of laponite: New insights into the ageing phenomena,” *Proc. R. Soc. A: Math. Phys. Sci.* **464**, 469–489 (2007).
- [7] Ewoldt, R. H., M. T. Johnston, and L. M. Caretta, “Experimental challenges of shear rheology: How to avoid bad data,” in *Complex Fluids in Biological Systems*, edited by S. Spagnolie (Springer, New York, 2015).
- [8] Hudson, R. E., A. J. Holder, K. M. Hawkins, P. R. Williams, and D. J. Curtis, “An enhanced rheometer inertia correction procedure (ERIC) for the study of gelling systems using combined motor-transducer rheometers,” *Phys. Fluids* **29**, 121602 (2017).
- [9] Baravian, C., G. Benbelkacem, and F. Caton, “Unsteady rheometry: Can we characterize weak gels with a controlled stress rheometer?,” *Rheol. Acta* **46**, 577–581 (2007).
- [10] Arigo, M. T., and M. T. McKinley, “The effects of viscoelasticity on the transient motion of a sphere in a shearthinning fluid,” *J. Rheol.* **41**, 103–128 (1997).
- [11] Lauger, J., and H. Stettin, “Effects of instrument and fluid inertia in oscillatory shear in rotational rheometers,” *J. Rheol.* **60**, 393–406 (2016).
- [12] Schrag, J. L., “Deviation of velocity gradient profiles from the ‘gap loading’ and ‘surface loading’ limits in dynamic simple shear experiments,” *Trans. Soc. Rheol.* **21**, 399–413 (1977).
- [13] Krieger, I., “The role of instrument inertia in controlled stress rheometers,” *J. Rheol.* **34**, 471–483 (1990).
- [14] Wylie, C. R., and L. C. Barret, *Advanced Engineering Mathematics*, 6th ed. (McGraw Hill, New York, 1995).
- [15] Ferry, J. D., *Viscoelastic Properties of Polymers*, 3rd ed. (Wiley, New York, 1980).
- [16] Whorlow, R. W., *Rheological Techniques*, 1st ed. (Ellis Horwood, New York, 1980).
- [17] Hu, Y. T., C. Palla, and A. Lips, “Comparison between shear banding and shear thinning in entangled micellar solutions,” *J. Rheol.* **52**, 279–400 (2008).
- [18] Cheng, P., M. C. Burroughs, G. L. Leal, and M. E. Helgeson, “Distinguishing shear banding from shear thinning in flows with a shear stress gradient,” *Rheol. Acta* **56**, 1007–1032 (2017).
- [19] Geri, M., B. Keshavarz, T. Divoux, C. Clasen, D. J. Curtis, and G. H. McKinley, “Time-resolved mechanical spectroscopy of soft materials via optimally windowed chirps,” *Phys. Rev. X* **8**, 041042 (2018).
- [20] Curtis, D. J., A. Holder, N. Badii, J. Claypole, M. Walters, B. Thomas, M. Barrow, D. Deganello, M. R. Brown, P. R. Williams, and K. Hawkins, “Validation of optimal Fourier rheometry for rapidly gelling materials and its application in the study of collagen gelation,” *J. Non-Newtonian Fluid Mech.* **222**, 253–259 (2015).